A Mathematical Model of Cellular Senescence

Yuhan Xiao   Mohamad Bairakdar

Abstract

Senescent cells are important biological factors that impact human mortality and morbidity rates. Removing senescent cells from the body of model organisms like mice has shown promise as an effective anti-aging therapy. However, there have been few attempts to mathematically model the accumulation and trajectories of senescent cells with age. In this work, we analyze a recent model that simulates the progression of a heterogeneous population of cells towards cellular senescence. The model we analyze considers proliferative, growth-arrested, apoptotic, and senescent cells, but makes the simplifying assumption that growth-arrested cells do not transition back to the proliferative state. In an attempt to make the model more realistic, we extend it to allow such a scenario and model the transition using a uniform probability distribution. For both the original and extended models, parameter values are obtained using a genetic algorithm that fits the models to an *in vitro* human primary fibroblast dataset of experimental markers of senescence tracked over time. The code associated with this paper can be found at https://github.com/mdanb/senescence_model.

1   Introduction

Senescent cells accumulate in the body with age and play a direct role in biological aging. It has been shown that removal of these cells from the body in mice increases their lifespan by around 25%, and decreases the incidence of many age-related diseases including cancer, cardiovascular diseases, and neurodegenerative diseases, among others (Childs et al., 2015). That being said, senescent cells only make up a fraction of the population of aged cells in an adult. Other types of cells that can be found in an adult organism include proliferative, apoptotic, and reversibly growth arrested cells, which, unlike senescent cells, are not detrimental to health. This heterogeneity in the composition of the adult cell population makes it challenging to use biomarkers to track the population of senescent cells over time, as currently no such marker is specific to senescent cells. For instance, the biomarker γH2AX can identify senescent cells, but will also identify any cell exhibiting DNA damage. One possible way to overcome this challenge is to combine multiple biomarkers. However, this approach can be expensive and time-consuming (Galvis et al., 2019).

There has been so far little effort to build mathematical models of the accumulation of senescent cells with age. The importance of such models on the development of effective anti-aging, anti-senescent cell therapies cannot be overstated; modeling the trajectory of cells towards the senescent state while distinguishing these cells from other types of cells can allow researchers and clinical experts to gauge the effectiveness of new anti-senescent cell therapies. Moreover, combining biological knowledge, experimental data, and model assumptions can help deepen our understanding of the process of cellular aging. In practice, building a model of cell population numbers over time and comparing it to experimental data can also reduce costs of future cell senescence experiments by helping to determine the minimal amount of data that needs to be collected to build reliable models. Galvis et al. (2019)'s recent work is among the few that have attempted to come up with a mathematical model of cellular senescence that takes into account the dynamics of a heterogeneous cell population. Briefly, the authors bucket aging cells into one of four categories: proliferative, senescent, apoptotic, and (reversibly) growth arrested. They then take a dynamical systems approach to model the evolution of the cell population with time. They fit their model to a human fibroblast experimental dataset of the amount of five experimental markers of senescence: the total number of population doublings, and the four biomarkers SA-β-Gal, γH2AX, Ki-67, and TUNEL. They find that the model is able to accurately capture the evolution of these senescence markers. Nonetheless, the authors do not consider the possibility of cells that have entered the growth arrested state to re-enter the proliferative state. We thus

extend and analyze a model that does account for such a possibility. The **main contributions** of our work are the following:

1. We extend the model presented in (Galvis et al., 2019) to take into account cells that re-enter the proliferative state after entering (reversible) growth arrest

2. We determine and compare the steady states of the original and extended model, as well as their stability

2 Background

In this section, we provide the biological background that is necessary to understand our paper, and elaborate on the model that is adopted in Galvis et al. (2019). In particular, we discuss the four different cell states that cells can enter: proliferative, senescent, apoptotic, and growth arrested. We highlight the difference between senescent, apoptotic, and growth arrested cells. To do the latter, we mainly summarize the key points from Blagosklonny (2011), which we refer the reader to for more details.

2.1 Biological Background

2.1.1 Living cells: Proliferative, Growth arrested, and Senescent cells

Senescent cells are cells that accumulate in the body with age. In adults, most cells are growth arrested but are non-senescent. Cells can enter the growth arrested state from the proliferative state - the state where cells can still divide - when, among other possibilities, serum growth factors and nutrients are no longer produced by the body. Cells that are growth arrested are said to be "quiescent." Although growth arrested cells do not divide i.e do not undergo the cell cycle, they still exhibit metabolic functions and synthesize proteins, albeit at a reduced rate. Similar to growth arrested cells, senescent cells also no longer divide and exhibit metabolic functions. However, unlike the growth arrested state, which is reversible, the senescent state is irreversible. In other words, once a cell enters the growth arrested state, it is able to transition back to the proliferative state. In contrast, once a cell enters the senescent state, it can no longer go back. Additionally, the reason that cell cycle arrest occurs is different between growth arrested and senescent cells. As previously mentioned, growth arrested cells do not divide because growth stimulation is no longer induced. Senescent cells are actually stimulated to grow by growth stimulating pathways like mTOR and MAPK. Thus, in the case of senescent cells, cell cycle arrest can only happen if other factors inhibit it. For instance, protein kinases like CDK which play a role in the cell cycle may be inhibited by CDK inhibitors including p21, p16, and p57. These inhibitors have no effect on the growth promoting pathways and thus growth stimulation persists despite cell cycle arrest. After some time of this conflict between growth stimulation and inhibition, the cell loses its ability to divide irreversibly, so that even when cell cycle inhibitors are withdrawn, the cell can no longer proliferate (Blagosklonny, 2011).

A useful "car driving" analogy has been presented by Blagosklonny (2011) to help understand the proliferative, growth arrested, and senescent cell states. The proliferative state is essentially like pushing the gas pedal and allowing the car to move. The "gas" in this case is analogous to, for example, serum growth factors that stimulate the growth and proliferation of cells. The growth arrested state is analogous to removing one's foot off the gas pedal, so cells no longer divide. The senescent state is like pushing the gas pedal while simultaneously pushing the brakes. In this sense, the senescent state is destructive. These three different scenarios are illustrated in Figure 1, A, B, and C respectively.
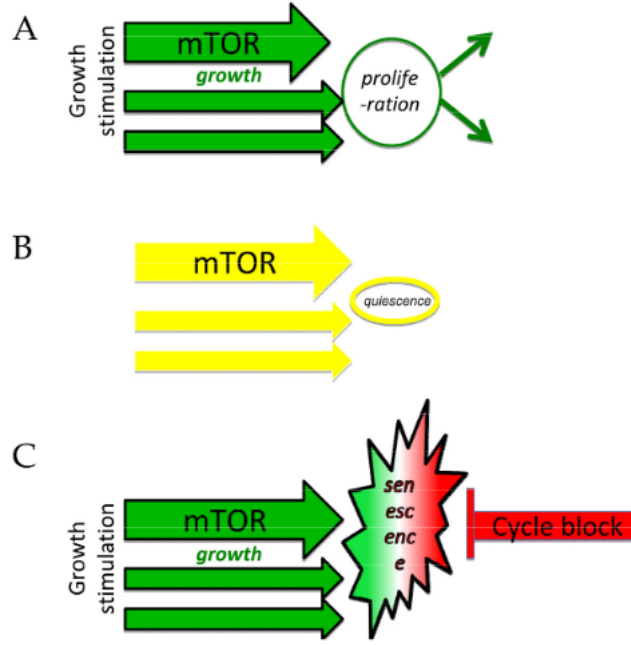
Figure 1: **(A)** Proliferating cells. Growth stimulation causes cells to undergo the cell cycle. **(B)** Growth stimulating pathways like mTOR are deactivated. Cells become quiescent and do not undergo the cell cycle. **(C)** Growth stimulation is induced at the same time as cell cycle blockage. This causes cells to enter the senescent state. Taken from Blagosklonny (2011).

2.1.2 Dead cells: Apoptotic cells

So far, we have discussed three types of cell states, all of which were states where the cell was still "alive". One more cell state that is relevant to our discussion is the apoptotic state. This is essentially cell death. Unlike in senescence, once a cell enters the apoptotic state and subsequently dies, it no longer exhibits metabolic functions. Cells that die normally through the process of apoptosis are not quite destructive. Notably, senescent cells have been speculated to have tumor promoting properties, particularly at old age, while apoptosis has mostly been shown to be a mechanism that prevents cells from turning cancerous (Childs et al., 2014).

2.2 Modeling approach taken by Galvis et al. (2019)

We now turn our attention to describing the modeling approach taken by Galvis et al. (2019).

2.2.1 Preliminaries

We begin by introducing nomenclature we use in the rest of the paper. This section should be referred to for any symbols that are used subsequently in the paper if need be. We define the following shorthand: G (growth arrested cells), A (apoptotic cells), S or P_N (senescent cells), D (dead cells, removed from the system), TP (total population = P + G + S + A), X (arbitrary model population), $m_{X_1 X_2}$ (rate for the transition from X_1 to X_2), PD (number of population doublings), Y (arbitrary experimental marker, of which there are 5: the 4 biomarkers SA-β-Gal, γH2AX, Ki-67, and TUNEL, and the experimental marker PD), U_{model} (if U is a cell population e.g P or G or A or S, prediction by the model of the proportion of cells in the population that are of type U. If U is a biomarker, prediction by the model of the proportion of cells, regardless of type, that express biomarker U), $TP_{model} = P_{model} + G_{model} + S_{model} + A_{model}$ (total number of cells predicted by the model), M (total number of cell passages i.e subcultures. Measurements are made at each cell passage so cell passages can be thought of in this context as data collecting time-points), PD_{model} (total population doublings predicted by model), PD_{data} (total population doublings from experimental data), U_{data} (the proportion of cells, regardless of type, that express biomarker U according to the experimental data). All parameters used in this paper are positive.

2.2.2 Model overview

Figure 2 shows a schematic of the dynamics of cellular aging, and helps inform the model equations that were adopted by the authors. Notice that at each proliferative state P_i, except for $i = N - 1$, cells have four possible states that they can move to: P_{i+1}, $P_N|S$, G, or A. Here, N represents the Hayflick limit, the maximum number of times a cell can divide before reaching the senescent state. N is assumed to be 50 by the authors, and they find that their model is robust to changes to the value of N. If a cell exits a given proliferative state and enters the next proliferative state, it enters as two cells due to mitosis. Thus, cells leaving state i at some rate enter the next proliferative state at twice that rate. At proliferative state i, the cell is said to have a *doubling age* of i; that is, it has divided i times so far. Moreover, notice that at any given proliferative state, the cell can jump directly to the senescent state without undergoing further cell division. Thus, cells entering the senescent state from a given state enter at the same rate that they leave that state. For the same reason, cells entering or leaving the growth arrested or apoptotic state at a rate r enter or leave that state at the same rate r. For $i = N - 1$, cells have not four possible directions to move in, but three, since the succeeding proliferative state is not actually proliferative: it is the senescent state. A subtlety that is worth noting is that for $i = N - 1$, cells can enter the senescent state at either double the rate that the leave state P_i or at the same rate. This is because cells in this state could actually turn senescent before dividing one last time.

We might expect that as cells progress towards senescence i.e as their doubling age increases, the rates at which they jump directly to the senescent state and to the apoptotic state would increase because the accumulation of DNA damage over the life-course of the cell can cause it to become senescent before dividing N times. Similarly, we might expect that the rate at which they transition to the growth arrested state would also increase, due to factors like signalling from senescent cells. Finally, we might expect the rate at which they transition to the next proliferative state to decrease, due to the slowing of cellular movement. While all the previous assertions make sense logically, in practice, the authors only assume that these rates are linearly proportional to doubling age, without assuming an increasing or decreasing relationship. Assuming a linear relationship effectively means that once these rates are determined for the first and last states, they are known for all intermediate states. For instance, once $m_{P_0 P_1}$ and $m_{P_{N-1} P_N}$ are known, all of $m_{P_i P_{i+1}}$ are known for $i = 1, ..., N-2$. Additionally, note that, in this model, once a cell enters the growth arrested state, it cannot transition back to the proliferative state, but only to the senescent state. This is a simplifying assumption that the authors make, since as described previously, the growth arrested state is in fact reversible.
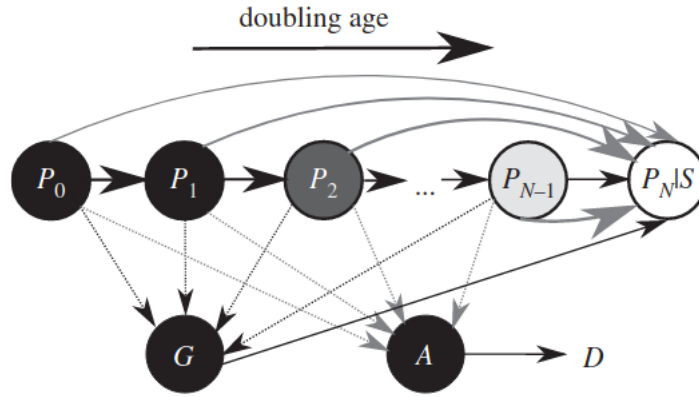
Figure 2: An illustration of the dynamics of cellular aging. P_i represents proliferative state i, the state a cell enters after having divided i times. P_N or S represents the senescent state, G the growth arrested state, and A followed by D the apoptotic state followed by cell death. The arrows going out of a given state represent the possible states that a cell can move towards from that state. The doubling age represents the age of a cell in terms of the number of times it has divided. See text for description of the dynamics. Taken from Galvis et al. (2019).

2.2.3 Model equations and parameters

The model equations are given below.

$$\frac{dP_0}{dt} = -(m_{P_0 P_1} + m_{P_0 S} + m_{P_0 A} + m_{P_0 G})P_0 \tag{1}$$

$$\frac{dP_i}{dt} = 2m_{P_{i-1} P_i} P_{i-1} - (m_{P_i P_{i+1}} + m_{P_i S} + m_{P_i A} + m_{P_i G})P_i \qquad \text{for i=1...}N-1 \tag{2}$$

$$\frac{dS}{dt} = \frac{dP_N}{dt} = 2m_{P_{N-1} P_N} P_{N-1} + \sum_{i=0}^{N-1} m_{P_i S} P_i + m_{GS} G \tag{3}$$

$$\frac{dG}{dt} = -m_{GS} G + \sum_{i=0}^{N-1} m_{P_i G} P_i \tag{4}$$

$$\frac{dA}{dt} = -m_{AD} A + \sum_{i=0}^{N-1} m_{P_i A} P_i \tag{5}$$

$$P = \sum_{i=0}^{N-1} P_i \tag{6}$$

$$TP = P + G + S + A \tag{7}$$

Equation 1 describes the rate of change of the initial proliferative population P_0. Cells can only leave this population, with a rate proportional to P_0. The transition rates are denoted as $m_{X_1 X_2}$, which describes cells jumping from population X_1 to X_2. For example, $m_{P_0 P_1}$ is the transition rate from the initial proliferative sub-population P_0 to the next proliferative population P_1.

Equation 2 describes the rate of change of the proliferative population P_i, where i ranges from 1 to $N-1$. Cells can leave this population at a rate proportional to P_i. New cells can enter this population through mitosis of cells in P_{i-1}.

Equation 3 describes the rate of change of the senescent cell population P_N or S. Cells can enter this population through mitosis of cells in P_{N-1}, from any other proliferative populations at a rate proportional to P_i where i ranges from 0 to $N-1$, or from the growth-arrested population at a rate of m_{GS}. Note the distinction between $m_{P_{N-1} P_N}$ and $m_{P_{N-1} S}$: the former corresponds to cells that divide a maximum number of times N, while the latter represents cells that turn senescent after dividing $N-1$ times, when they could still undergo one more division.

Equation 4 describes the rate of change of the growth-arrested cell population G. Cells can leave this population to enter the senescent state at a rate of m_{GS} or enter this population from any proliferative population P_i, at a rate of $m_{P_i G}$, where i ranges from 0 to $N-1$.

Equation 5 describes the rate of change of the apoptotic cell population A. Cells can die and leave this population at a rate of m_{AD} or enter this population from any proliferative population P_i at a rate of $m_{P_i A}$, where i ranges from 0 to $N-1$.

Equation 6 says that the total proliferative population P equals to the sum of each proliferative sub-populations P_i where i ranges from 0 to $N-1$.

Equation 7 says that the total population of cells equals to the sum of the total proliferative, growth-arrested, senescent, and apoptotic cell populations.

In Table 1, we list the parameters associated with the model, of which there are 14. The last three parameters are discussed in section 2.2.4. They do not appear in the system of differential equations, but appear in the error function that is used for optimization/data fitting. In Figure 3, we show transition rates of cells from/to different cell states. These are obtained through optimization, as described in Section 2.2.4. As mentioned previously, these are assumed to depend linearly on doubling age. The expectations of Galvis et al. (2019) regarding how these rates depend on cell doubling age, described in Section 2.2.2, are mostly met: we see that transition rates between one proliferative state to the next decrease with doubling age, while rates for the transitions from the proliferative state to the growth arrested and senescent states increase with doubling age. The only unexpected result is that the rate of transition from proliferative states to the apoptotic state mostly remains constant with doubling age, and even decreases very slightly.

Parameter	Units	Value
$m_{P_0 P_1}$	h^{-1}	0.0265
$m_{P_{N-1} P_N}$	h^{-1}	0.0057
$m_{P_0 P_G}$	h^{-1}	0.0022
$m_{P_{N-1} P_G}$	h^{-1}	0.0031
$m_{P_0 P_S}$	h^{-1}	0.0027
$m_{P_{N-1} P_S}$	h^{-1}	0.0052
$m_{P_0 P_A}$	h^{-1}	0.0018
$m_{P_{N-1} P_A}$	h^{-1}	0.0016
m_{GS}	h^{-1}	6.837×10^{-4}
m_{AD}	h^{-1}	0.0011
N	# of divisions	50
$P_{\gamma H2AX}$	%	23.05
G_{Ki-67}	%	99.96
$G_{\gamma H2AX}$	%	85.12

Table 1: Free model parameters. h represents hours. All parameters are obtained through optimization except for N, whose value is pre-set to 50. The optimized values here are based on our runs of the authors' code rather than the values reported in the original manuscript. We ran the optimization algorithm using 5 random seeds and report the parameter values obtained from the seed that resulted in the lowest total data fit error. Notice that the transition rate from proliferative states to apoptotic state mostly remain constant with doubling age
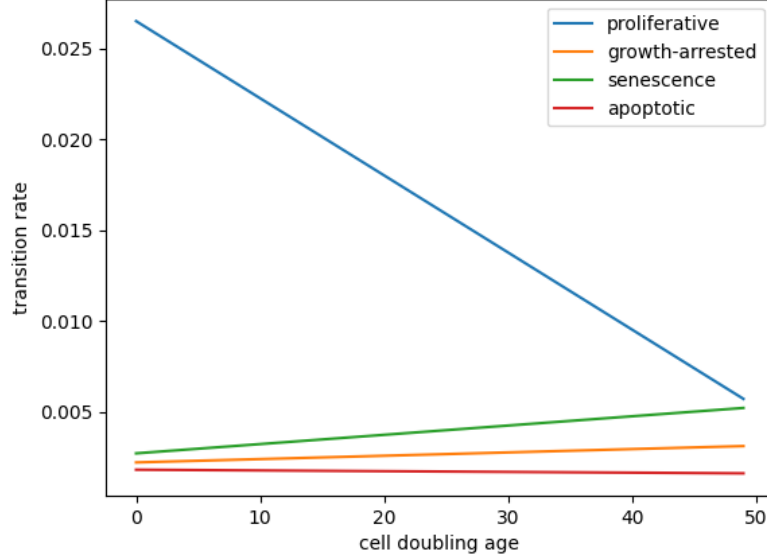
Figure 3: Plot showing how the transition rates from/to different cell states change with cell doubling age. As mentioned in the text, these rates are assumed to have a linear dependency on doubling age.

2.2.4 Data fitting

The authors fit their model to experimental biomarker data collected over 16 human fibroblast cell passages using a genetic algorithm. The biomarkers used are SA-β-Gal, γH2AX, Ki-67, and TUNEL. The following **simplifying** assumptions are made about the proportion of the different cells expressing these biomarkers (we stress simplifying because recall, current biomarkers are not exclusively expressed by a single type of cell):

- SA-β-Gal maps exclusively to senescent cells

- TUNEL maps exclusively to apoptotic cells

- Ki-67 maps to proliferative cells and to a fraction of growth arrested cells

- γH2AX maps to the entire population of senescent and apoptotic cells and to a fraction of proliferative and growth-arrested cells.

The fact that the last two biomarkers are assumed to map to multiple types of cells incites the introduction of parameters to model these proportions. Since these proportions are not known, they are obtained through optimization. These parameters are denoted by $P_{\gamma H2AX}$, G_{Ki-67}, and, $G_{\gamma H2AX}$. The first of these parameters represents the proportion of proliferative cells that express the biomarker $\gamma H2AX$ at any given time. Similarly, the second and third parameters represent the proportion of growth arrested cells that express the biomarkers $Ki-67$ and $\gamma H2AX$ respectively. The outputs of the model's system of differential equations are the populations of each type of cell, which can be converted into percentages by dividing by TP_{model}. For data fitting purposes, it is necessary to compare model predictions to the actual experimental data. Given that model outputs represent percentages of specific cell types, while the experimental data measures the proportion of cells that express a given biomarker among the total population of cells, it is necessary to convert the former to the latter. This is done as follows.

$$Ki - 67_{model} = \frac{P_{model} + G_{Ki-67}G_{model}}{TP_{model}}$$

$$\gamma H2AX_{model} = \frac{S_{model} + A_{model} + G_{\gamma H2AX}G_{model} + P_{\gamma H2AX}P_{model}}{TP_{model}}$$

$$SA - \beta - Gal_{model} = \frac{S_{model}}{TP_{model}}$$

$$TUNEL_{model} = \frac{A_{model}}{TP_{model}}$$

Note that the fraction of cells expressing $Ki-67$ predicted by the model is equal to the predicted proportion of cells that make up the proliferative population, and a fraction of the predicted proportion of cells that make up the growth arrested population. Similar logic applies to the remaining biomarker model predictions. Furthermore, note that the model also monitors the total population of cells over time (See Equation 7). From this, one can then compute the total number of times the population of cells is predicted to have doubled at any given point in time t according to the model, using the equation: $PD(t)_{model} = log_2 \frac{TP(t)_{model}}{TP(0)_{model}}$. This can then be compared to $PD(t)_{data}$ for different values of t. Taking into account population doublings in this way can allow the model to be more faithful to actual cell growth kinetics.

The following cost function was used for data fitting purposes:

$$Error = \sqrt{\sum_Y \sum_{i=1}^M (\frac{Y_{data_i} - Y_{model_i}}{\max_j Y_{data_j}})^2}$$

Here, i represents the index for a given cell passage e.g $i = 1$ represents passage 1. M represents the total number of cell passages at which the authors made measurements and is equal to 16.

3 Analysis of the model in Galvis et al. (2019)

In this section, we perform a steady state analysis of the model given in Galvis et al. (2019), whose equations we have presented in section 2.2.3.

3.1 What are the steady states?

We begin by finding the steady states.

$$\frac{dP_0}{dt} = -(m_{P_0 P_1} + m_{P_0 S} + m_{P_0 A} + m_{P_0 G})P_0$$
$$= 0$$
$$\Rightarrow P_0 = 0$$

$$\frac{dP_i}{dt} = 2m_{P_{i-1}P_i}P_{i-1} - (m_{P_iP_{i+1}} + m_{P_iS} + m_{P_iA} + m_{P_iG})P_i \qquad \text{for i=1...}N-1$$
$$= 0$$

$$2m_{P_{i-1}P_i}P_{i-1} - (m_{P_iP_{i+1}} + m_{P_iS} + m_{P_iA} + m_{P_iG})P_i = 0$$

$$2m_{P_{i-1}P_i}P_{i-1} = (m_{P_iP_{i+1}} + m_{P_iS} + m_{P_iA} + m_{P_iG})P_i$$

$$\frac{2m_{P_{i-1}P_i}P_{i-1}}{(m_{P_iP_{i+1}} + m_{P_iS} + m_{P_iA} + m_{P_iG})} = P_i$$

We compute P_1 first:

$$P_1 = \frac{2m_{P_0P_1}P_0}{(m_{P_1P_2} + m_{P_1S} + m_{P_1A} + m_{P_1G})}$$
$$= \frac{2m_{P_0P_1} \times 0}{(m_{P_1P_2} + m_{P_1S} + m_{P_1A} + m_{P_1G})}$$
$$= 0$$

By the same logic, $P_i = 0$ for all i=2...$N-1$

$$\frac{dG}{dt} = -m_{GS}G + \sum_{i=0}^{N-1} m_{P_iG}P_i$$
$$= 0$$

$$m_{GS}G = \sum_{i=0}^{N-1} m_{P_iG}P_i$$

$$G = \frac{\sum_{i=0}^{N-1} m_{P_iG}P_i}{m_{GS}}$$
$$= \frac{\sum_{i=0}^{N-1} m_{P_iG} \times 0}{m_{GS}}$$
$$= 0$$

$$\frac{dS}{dt} = \frac{dP_N}{dt} = 2m_{P_{N-1}P_N}P_{N-1} + \sum_{i=0}^{N-1} m_{P_iS}P_i + m_{GS}G$$
$$= 0$$

Since $P_i = 0$ for all i=0,...,$N-1$ and $G = 0$ at steady state, we do not obtain any new information from this equation.

$$\frac{dA}{dt} = -m_{AD}A + \sum_{i=0}^{N-1} m_{P_iA}P_i$$
$$= 0$$

$$m_{AD}A = \sum_{i=0}^{N-1} m_{P_iA}P_i$$

$$A = \frac{\sum_{i=0}^{N-1} m_{P_iA}P_i}{m_{AD}}$$
$$= \frac{\sum_{i=0}^{N-1} m_{P_iA} \times 0}{m_{AD}}$$
$$= 0$$

$$TP = P + G + S + A$$

$$S = TP - P - G - A$$

$$= TP$$

Thus, we obtain a single steady state $(\bar{P}_0, ..., \bar{P}_N, \bar{G}, \bar{A}, \bar{S}) = (0, ..., 0, 0, 0, TP)$

3.2 Steady state stability analysis

We now examine the stability of the steady state we obtained. We compute the Jacobian associated with our system of equations. Because of Equation 7, we can eliminate the senescent state equation $\frac{dS}{dt}$ from our analysis of the Jacobian, and analyze stability excluding the variable S. We can then use Equation 7 to determine the stability of the steady state which includes the variable S. We use the following notation: $\alpha_i = -(m_{P_i P_{i+1}} + m_{P_i S} + m_{P_i A} + m_{P_i G})$, $\beta_i = 2m_{P_{i-1} P_i}$, $\gamma_i = m_{P_i G}$, and $\delta_i = m_{P_i A}$.

$$J = \begin{array}{c}
\begin{array}{ccccccccc} P_0 & P_1 & P_2 & P_3 & \ldots & P_{N-2} & P_{N-1} & G & A \end{array} \\
\begin{pmatrix}
\alpha_0 & 0 & 0 & 0 & \ldots & 0 & 0 & 0 & 0 \\
\beta_1 & \alpha_1 & 0 & 0 & \ldots & 0 & 0 & 0 & 0 \\
0 & \beta_2 & \alpha_2 & 0 & \ldots & 0 & 0 & 0 & 0 \\
\vdots & & \ddots & \ddots & \ddots & \vdots & \vdots & \vdots & \vdots \\
0 & 0 & 0 & 0 & \ldots & \beta_{N-1} & \alpha_{N-1} & 0 & 0 \\
\gamma_0 & \gamma_1 & \gamma_2 & \gamma_3 & \ldots & \gamma_{N-2} & \gamma_{N-1} & -m_{GS} & 0 \\
\delta_0 & \delta_1 & \delta_2 & \delta_3 & \ldots & \delta_{N-2} & \delta_{N-1} & 0 & -m_{AD}
\end{pmatrix}
\end{array}
\begin{array}{c}
\frac{dP_0}{dt} \\
\frac{dP_1}{dt} \\
\frac{dP_2}{dt} \\
\vdots \\
\frac{dP_{N-1}}{dt} \\
\frac{dG}{dt} \\
\frac{dA}{dt}
\end{array}$$

We note that the Jacobian is lower triangular, so the eigenvalues are the diagonal entries i.e the eigenvalues are $\alpha_0, ..., \alpha_{N-1}, -m_{GS}$, and $-m_{AD}$. All of the eigenvalues are negative, which implies the steady state $(\bar{P}_0, ..., \bar{P}_N, \bar{G}, \bar{A}) = (0, ..., 0, 0, 0)$ is stable. Since P_i is 0 for $i = 0, ..., N-1$ at steady state, no cells are dividing and creating new cells. Since $A = 0$ at steady state, no cells are dying and leaving the population. Thus, at steady state, TP is a constant. Hence, S = TP is a constant. So S is also stable at steady state. This leads to the conclusion that the steady state $(\bar{P}_0, ..., \bar{P}_N, \bar{G}, \bar{A}, \bar{S}) = (0, ..., 0, 0, 0, TP)$ is stable. We confirm these results graphically by plotting the evolution of the cell populations with time. We fit the model to the data and obtain the parameters listed in Table 1. In Figure 4 (a)-(e), the model predictions are compared to the experimental marker data. In Figure 4 (f), the model's predictions of the fraction of each cell type (P, A, G, and S) across the whole population is shown over time. Indeed, we observe that eventually, all cell types die out except for the senescent population.
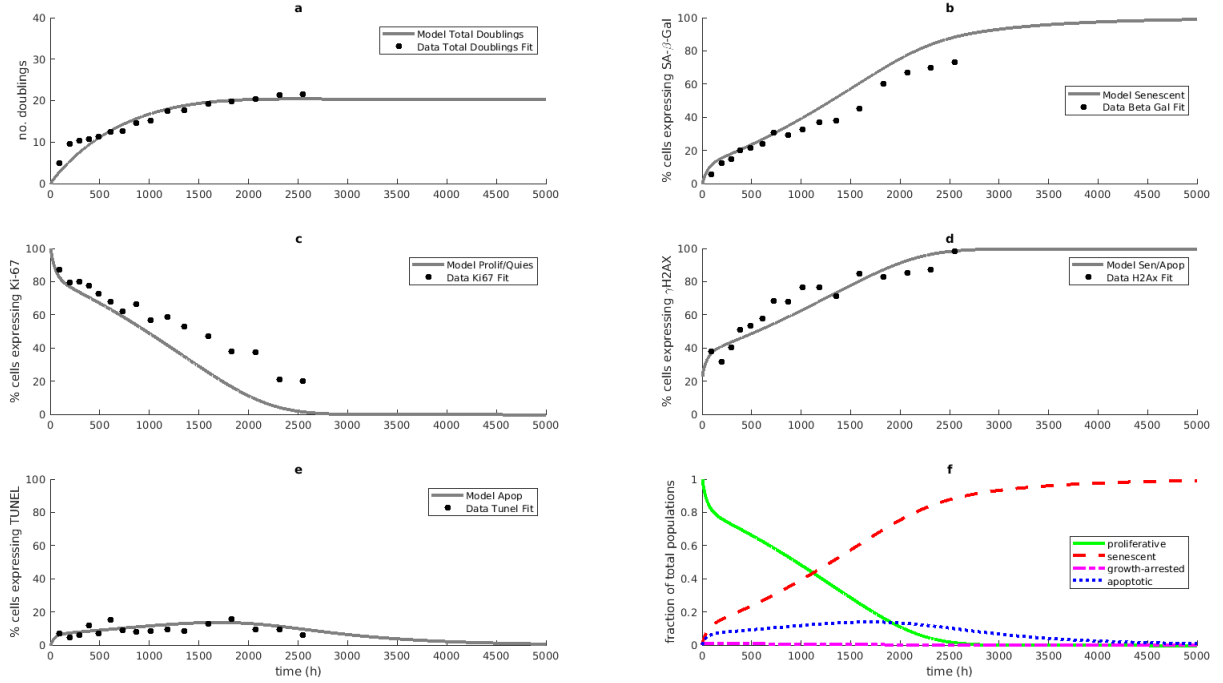
Figure 4: (a)-(e) Experimental marker data versus model predictions. (f) model predictions of the fraction of cells of each type (P, A, G, S) over time. In (a), the model predictions of the number of times the population of cells doubles are compared to experimental population data. In (b)-(e), the model predictions of the percentage of cells expressing SA-β-Gal, Ki-67, $\gamma H2AX$, and TUNEL respectively are compared to the corresponding percentages from the experimental data. We note that in (f), the growth arrested population fraction appears to be 0 initially, but this is simply because the fraction of growth arrested cells is small relative to other cell types.

4 A Potentially Improved Model

4.1 Model Extension

As previously mentioned, Galvis et al. (2019) make the assumption that cells cannot go from the growth arrested state back to any of the proliferative states. In practice, this indeed may occur. Thus, we extend their model to take into account this possibility. We expect our model to fit the data better since it is truer to the underlying biology while making no simplifications to the original model. In being more true to the biology, we expect to be able to draw more realistic conclusions from the model. Ultimately, having a more realistic model may help us gain a better understanding of the trajectory of cells towards senescence. As we shall describe next, we only add a single extra parameter to the model, which implies that we do not over-parametrize the model relative to the previous one, so the comparison between the models is more or less fair[1]. There exists a challenge in extending the model as proposed, however; once a cell enters the growth-arrested state from some proliferative state, it is not possible to distinguish this cell from cells entering the growth arrested state from other proliferative states. Thus, it is necessary to model the transition back to proliferative states probabilistically. We make the simplifying assumption that cells transition from the growth arrested state to any proliferative state in a uniformly distributed manner. We take $N = 50$ as in the original model, which implies that growth arrested cells transition to proliferative state i with probability $Pr(i) = \frac{1}{50}$. Finally, we introduce a new parameter k that describes the rate of transitioning out from the growth arrested state to any of the proliferative states. Our extended model is given by the equations below.

$$\frac{dP_0}{dt} = -(m_{P_0 P_1} + m_{P_0 S} + m_{P_0 A} + m_{P_0 G})P_0 + \frac{1}{50}kG \tag{8}$$

---

[1]it is possible to be more rigorous by comparing the models using a statistical analysis that takes into account degrees of freedom for each model, but this is beyond the scope of this work

$$\frac{dP_i}{dt} = 2m_{P_{i-1}P_i}P_{i-1} - (m_{P_iP_{i+1}} + m_{P_iS} + m_{P_iA} + m_{P_iG})P_i + \frac{1}{50}kG \qquad \text{for i=1...}N-1 \qquad (9)$$

$$\frac{dS}{dt} = \frac{dP_N}{dt} = 2m_{P_{N-1}P_N}P_{N-1} + \sum_{i=0}^{N-1} m_{P_iS}P_i + m_{GS}G \qquad (10)$$

$$\frac{dG}{dt} = -m_{GS}G + \sum_{i=0}^{N-1} m_{P_iG}P_i - kG \qquad (11)$$

$$\frac{dA}{dt} = -m_{AD}A + \sum_{i=0}^{N-1} m_{P_iA}P_i \qquad (12)$$

$$P = \sum_{i=0}^{N-1} P_i \qquad (13)$$

$$TP = P + G + S + A \qquad (14)$$

4.2 What are the steady states of the extended model?

We begin by solving the equation involving $\frac{dS}{dt}$ as it will simplify further calculations.

$$\frac{dS}{dt} = \frac{dP_N}{dt} = 2m_{P_{N-1}P_N}P_{N-1} + \sum_{i=0}^{N-1} m_{P_iS}P_i + m_{GS}G$$

$$= 0$$

$$-2m_{P_{N-1}P_N}P_{N-1} - m_{GS}G = \sum_{i=0}^{N-1} m_{P_iS}P_i$$

$$-(2m_{P_{N-1}P_N}P_{N-1} + m_{GS}G) = \sum_{i=0}^{N-1} m_{P_iS}P_i$$

$$\Rightarrow P_i = 0 \text{ for i=0,...,}N-1 \text{ and } G = 0$$

$$\frac{dG}{dt} = -m_{GS}G + \sum_{i=0}^{N-1} m_{P_iG}P_i - kG$$

$$= 0$$

Since $P_i = 0$ for all i=0,...,$N-1$ and $G = 0$ at steady state, we do not obtain any new information from this equation.

Since all other equations remain the same, we obtain the same steady state as in the original model: $(\bar{P}_0,..., \bar{P}_N, \bar{G}, \bar{A}, \bar{S}) = (0,..., 0, 0, 0, \text{TP})$.

4.3 Steady state stability analysis

We now examine the stability of the steady state we obtained. We compute the Jacobian associated with our system of equations. We use the same method and notation described in Section 3.2.

$$J = \begin{pmatrix}
\alpha_0 & 0 & 0 & 0 & \cdots & 0 & 0 & \frac{k}{50} & 0 \\
\beta_1 & \alpha_1 & 0 & 0 & \cdots & 0 & 0 & \frac{k}{50} & 0 \\
0 & \beta_2 & \alpha_2 & 0 & \cdots & 0 & 0 & \frac{k}{50} & 0 \\
\vdots & & \ddots & \ddots & \ddots & \vdots & \vdots & \vdots & \vdots \\
0 & 0 & \frac{k}{50} & 0 & \cdots & \beta_{N-1} & \alpha_{N-1} & \frac{k}{50} & 0 \\
\gamma_0 & \gamma_1 & \gamma_2 & \gamma_3 & \cdots & \gamma_{N-2} & \gamma_{N-1} & -m_{GS}-k & 0 \\
\delta_0 & \delta_1 & \delta_2 & \delta_3 & \cdots & \delta_{N-2} & \delta_{N-1} & 0 & -m_{AD}
\end{pmatrix}
\begin{matrix}
\frac{dP_0}{dt} \\
\frac{dP_1}{dt} \\
\frac{dP_2}{dt} \\
\vdots \\
\frac{dP_{N-1}}{dt} \\
\frac{dG}{dt} \\
\frac{dA}{dt}
\end{matrix}$$

with column headers $P_0 \quad P_1 \quad P_2 \quad P_3 \quad \cdots \quad P_{N-2} \quad P_{N-1} \quad G \quad A$

Unlike in the previous steady state stability analysis, obtaining the stability of the steady state in this case is not straightforward since the matrix is no longer lower triangular. Hence, we opt instead to analyze stability graphically.

We fit our new model to the experimental data using the approach described in Section 2.2.4. We run the algorithm using 5 different random seeds (instead of 20, as in Galvis et al. (2019), due to computational resource limitations) and pick the parameters that resulted in the lowest possible cost. We report these values in Table 2.

Parameter	Units	Value
$m_{P_0 P_1}$	h^{-1}	0.0222
$m_{P_{N-1} P_N}$	h^{-1}	0.0088
$m_{P_0 P_G}$	h^{-1}	7.85×10^{-4}
$m_{P_{N-1} P_G}$	h^{-1}	2.19×10^{-7}
$m_{P_0 P_S}$	h^{-1}	0.0014
$m_{P_{N-1} P_S}$	h^{-1}	0.0035
$m_{P_0 P_A}$	h^{-1}	0.0027
$m_{P_{N-1} P_A}$	h^{-1}	0.0083
m_{GS}	h^{-1}	0.05
m_{AD}	h^{-1}	0.0263
N	# of divisions	50
k	h^{-1}	3.71×10^{-4}
$P_{\gamma H2AX}$	%	39.35
G_{Ki-67}	%	53.47
$G_{\gamma H2AX}$	%	8.10×10^{-5}

Table 2: Free model parameters. h represents hours. All parameters are obtained through optimization except for N, whose value is pre-set to 50. The optimized values here are reported for the extended model. We ran the optimization algorithm using 5 random seeds and report the parameter values obtained from the seed that resulted in the lowest total optimization error.

In Figure 5, we show analogous graphs as those in Figure 4, except the data is fit using our extended model. What at first might seem surprising is that in 5 (a), we observe that the number of population doublings keeps increasing without bound. We elaborate on why this happens in Section 5. For now, we note that the model seems to graphically fit the data worse than the initial model. More concretely, we obtain a data fitting error of 1.0315, compared to an error of 0.8099 for the original model.
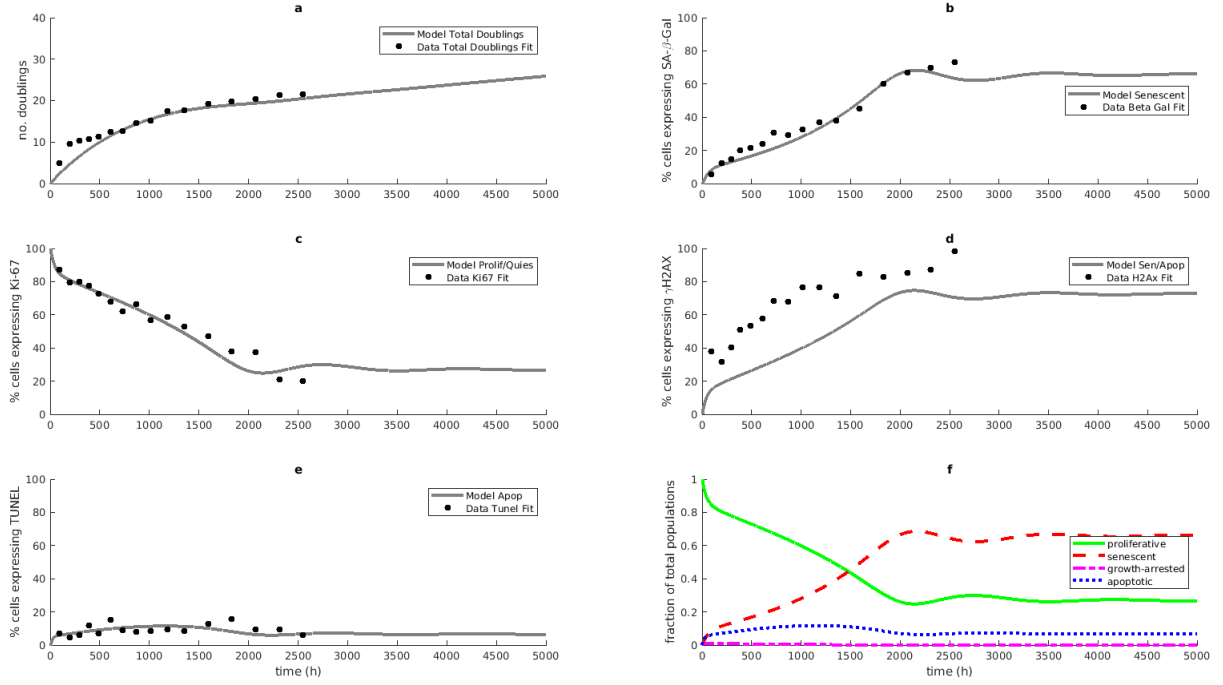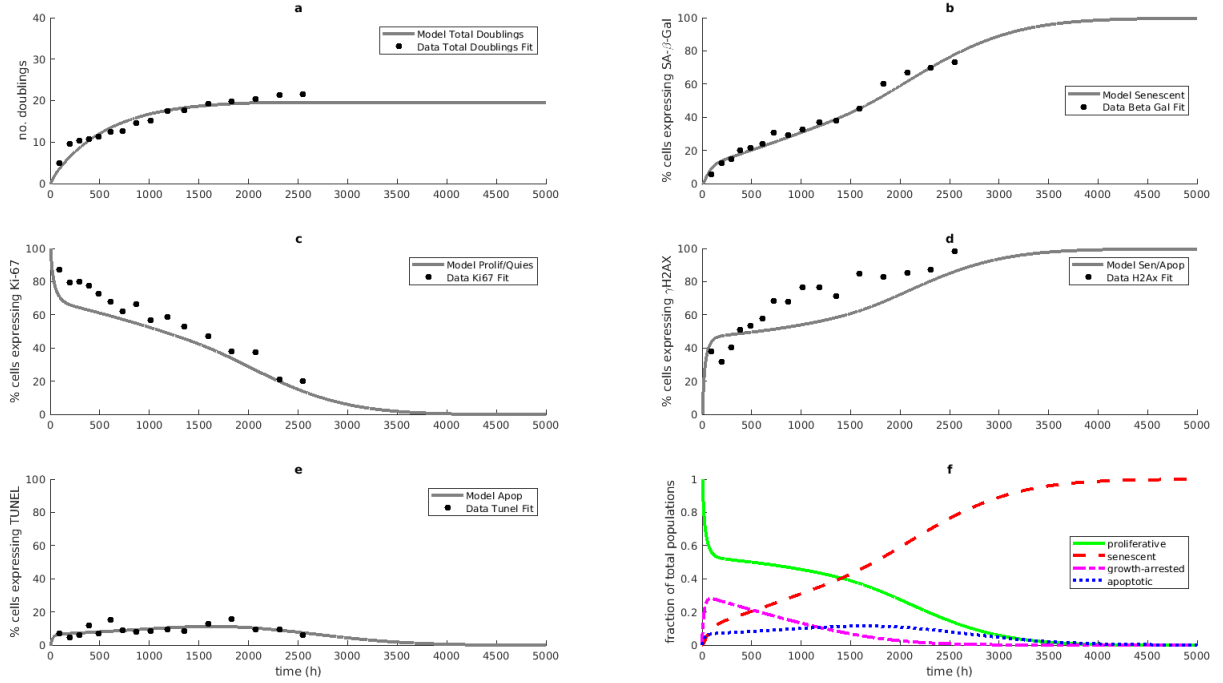
Figure 5: (a)-(e) Experimental marker data versus our model's predictions. (f) Our model's predictions of the fraction of cells of each type (P, A, G, S) over time with a uniform probability distribution for transition rate from growth-arrested state back to proliferative states. In (a), the model predictions of the number of times the population of cells doubles are compared to experimental population data. It shows that the cell population keeps doubling indefinitely i.e the populations of cells grows without bound. In (b)-(e), the model predictions of the percentage of cells expressing SA-β-Gal, Ki-67, $\gamma H2AX$, and TUNEL respectively are compared to the corresponding percentages from the experimental data. We note that our model does not fit the data well in (d). In (f), the growth arrested population fraction is not zero but just small relative to other cell types.

Our model shows that cell populations will grow unboundedly, which means that the steady state is not stable. The unexpected results we obtain warrant investigating why we observe this behavior. We thus change the distribution of cells returning from the growth-arrested state to the proliferative state from a uniform distribution to a discrete probability distribution that increases exponentially with doubling age. The equation that describes the new probability distribution is as follows:

$$prob(i) = \frac{2^i}{2^{50} - 1} \text{for i} = 0,...,49$$

We then run the optimization algorithm to obtain the graphs shown in Figure 6. As Figure 6 (a) shows, the number of times the population doubles eventually stops growing, as in Figure 4 (a). However, we also observe that the data is not better fit by our model than by the original model. Concretely, we obtain an error of 0.8116, which is slightly larger than the error obtained using the original model.

Figure 6: (a)-(e) Experimental marker data versus model predictions. (f) model predictions of the fraction of cells of each type (P, A, G, S) over time. In (a), the model predictions of the number of times the population of cells doubles are compared to experimental population data. The population eventually stops doubling and becomes constant. In (b)-(e), the model predictions of the percentage of cells expressing SA-β-Gal, Ki-67, $\gamma H2AX$, and TUNEL respectively are compared to the corresponding percentages from the experimental data. We note that in (f), proliferative, growth-arrested, and apoptotic cells eventually become extinct. Cell populations accumulate to a constant senescent state as total population stops doubling.

5 Discussion

The original model by Galvis et al. (2019) is quite accurate in capturing the complex dynamics of a heterogeneous aging cell population using a minimally parametrized model. The results are validated by examining how well the model fits experimental marker data. We extended the model in Galvis et al. (2019) to allow cells to transition from the growth arrested state back to the proliferative state after entering the growth arrested state, a scenario that the original model did not account for but that is very much viable in real cells. We expected that being truer to the biology would allow us to better fit the data and draw better conclusions from the model. We compared our extended model to the experimental data, and conclude that it does not reflect the evolution of cells towards cellular senescence as well as the original model.

We expected that our model which adopted a uniform probability distribution to describe the return of cells from the growth arrested state back to the proliferative state to have the same stable steady state as the one we have found in the original model. However, the graphical stability analysis in Figure 5 shows that our steady state is unstable. Cell populations increase without bound, which is not biologically sound. Upon further consideration of the model, we explain this behaviour by the fact that our model creates a loop that allows proliferative cells with a higher doubling age to transition back to earlier proliferative states, as shown in Figure 7. In other words, cells are essentially allowed to "travel back in time" and keep on dividing indefinitely. This loop is not biologically reasonable.
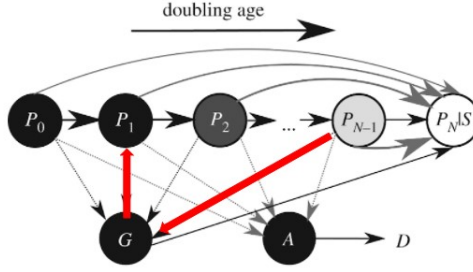
Figure 7: The creation of a loop as a result of a probability distribution that allows cells from later proliferative states to transition back to earlier proliferative states. In this example, growth-arrested cells coming from proliferative state P_{N-1} transition back to the much earlier proliferative state P_1, illustrated by red arrows.

Although not a solution to the loop problem, the model with a discrete probability distribution that increases exponentially with doubling age has a stable steady state. All cells eventually accumulate to a uniformly constant senescent population. This can be explained by the fact that this probability distribution minimizes the chances of cells traveling to very early proliferative states. We note that early proliferative states are the ones with the most potential to create a large number of new cells due to the exponential nature of cell doubling.

Given the findings regarding the sensitivity of the system to the probability distribution that is chosen, it would be interesting to examine more rigorously the relationship between the probability distribution and the behavior of the dynamics. However, since it is more pertinent to actually solve the loop problem, rather than to mitigate it, future modeling efforts should focus on finding a way to restrict movement from the growth-arrested state back to proliferative states in a biologically meaningful way. In particular, cells which enter the growth arrested state should only be allowed to transition back to the particular proliferative state that they came from.

Finally, we note that both our model and the original model lack a term to set a carrying capacity on cell growth. Biologically, there is a maximum amount of cells a body can sustain, and future efforts should take this into account.

References

Blagosklonny, M. V. (2011). Cell cycle arrest is not senescence. *Aging*, *3*(2), 94–101. https://doi.org/
 10.18632/aging.100281

Childs, B. G., Baker, D. J., Kirkland, J. L., Campisi, J., & Deursen, J. M. (2014). Senescence and
 apoptosis: Dueling or complementary cell fates? *EMBO reports*, *15*(11), 1139–1153. https:
 //doi.org/10.15252/embr.201439245

Childs, B. G., Durik, M., Baker, D. J., & van Deursen, J. M. (2015). Naturally occurring p16(ink4a)-
 positive cells shorten healthy lifespan. *Nature Medicine*, *21*(12), 1424–1435. https://doi.org/
 10.1038/nm.4000

Galvis, D., Walsh, D., Harries, L. W., Latorre, E., & Rankin, J. (2019). A dynamical systems model
 for the measurement of cellular senescence. *Journal of The Royal Society Interface*, *16*(159),
 20190311. https://doi.org/10.1098/rsif.2019.0311